(1965); 36, 217 (1966); Y. Hahn, *ibid.* 58, 137 (1970); 67, 389 (1971).

[3]Y. Hahn and L. Spruch, Phys. Rev. 153, 1159 (1967); Y. Hahn, Phys. Rev. C 1, 12 (1970).

[4]E. P. Wigner, Phys. Rev. 40, 749 (1932).

[5]A similar expression is of course available for the case of more than one particle (see Ref. 4).

[6]See, for example, R. Balescu, *Statistical Mechanics of Charged Particles* (Interscience, New York, 1963), Chap. 14.

[7]Planck's constant is retained in this section to explicitly exhibit classical and quantum aspects of our formulation.

[8]See, for example, N. F. Mott and H. S. W. Massey, *The Theory of Atomic Collisions* (Oxford U. P., London, 1965), Chap. 16.

[9]H. A. Bethe and E. F. Salpeter, in *Handbuch der Physik*, edited by S. Flügge (Springer, Berlin, 1957), Vol. 35.

[10]L. I. Schiff, *Quantum Mechanics* (McGraw-Hill, New York, 1955).

[11]C. J. Kleinman, Y. Hahn, and L. Spruch, Phys. Rev. 165, 53 (1968).

[12]M. L. Goldberger and K. M. Watson, *Collision Theory* (Wiley, New York, 1964), p. 303.

[13]Reference 12, p. 331.

PHYSICAL REVIEW A VOLUME 6, NUMBER 2 AUGUST 1972

Resonance-Narrowed-Lamb-Shift Measurement in Hydrogen, $n=3$†

C. W. Fabjan* and F. M. Pipkin
Lyman Laboratory, Harvard University, Cambridge, Massachusetts 02138
(Received 13 March 1972)

A new measurement of the Lamb shift in the $n=3$ state of atomic hydrogen is reported. The experiment was performed in zero magnetic field with a fast hydrogen beam. The radio-frequency spectroscopy measurements were made with both a single oscillating field and two separated oscillating fields. The final result for the Lamb shift was $\$(\mathrm{H}, n=3) = (314.819 \pm 0.048)$ MHz. In a further experiment, the separated-oscillating-field technique was used to narrow the resonance so that the linewidth was less than the natural linewidth.

I. INTRODUCTION

Precise measurements of the Lamb shift in hydrogenic atoms give one of the most sensitive tests of quantum electrodynamics.[1] The presently accepted theoretical value for the Lamb shift in the $n=2$ state of hydrogen agrees very well with the most recent measurements; it is calculated with a precision which is a factor of 5 greater than the experimental precision achieved to date.[2,3] Despite extensive experimental work, the precision of the measured value for the Lamb shift in the $n=2$ state of hydrogen has not been improved over that obtained by Lamb and his co-workers 20 years ago.[4,5] The new measurements significantly disagree with the older measurements.[5,6]

In these Lamb-shift measurements the width of the resonance is greater than or equal to the natural linewidth and it is determined essentially by the lifetime of the short-lived P state. Obtaining the stated one-standard-deviation precision requires determining the center of the resonance line to six parts in 10^4 of the natural linewidth. The natural linewidth imposes a fundamental limitation on the obtainable precision and a significant reduction of the experimental uncertainty will require a comparable reduction in linewidth.

This paper reports a measurement of the Lamb shift in the $n=3$ state of atomic hydrogen by a technique which uses the method of separated oscillating fields to narrow the resonance.[7,8] This technique was also used to show the feasibility of reducing the linewidth to less than the natural linewidth by selecting those atoms in which the P state lives longer than a mean life. The paper deals in succession with the principle of the experiment, the theory of the line shape, the apparatus, and the results.

II. PRINCIPLE OF THE EXPERIMENT

The reduction of the linewidth was performed with a technique familiar to molecular-beam spectroscopy which is known as the Ramsey separated-oscillating-field method.[9] The single Rabi-type interaction region used in earlier Lamb-shift measurements was replaced by two coherent rf fields separated by the distance L. Between the two rf regions the atoms spend a time $T=L/v$ in a field-free region. The linewidth is determined by T and the time spent in the two rf transition regions. The line can be made arbitrarily narrow by making T very long. Because of an interference effect between the S- and P-state wave functions, even when $T=0$ the linewidth is narrower than for a conventional Rabi-type rf system with the same over-all length. Since the mean life of a P state is quite short and the number of P states available for the interference measurement decreases as $e^{-\gamma_p T/2}$, where γ_p is the decay constant for the P state, the

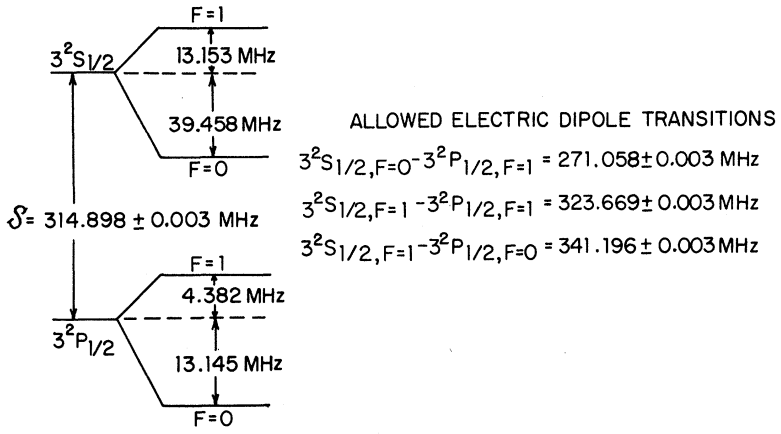

FIG. 1. Energy-level diagram for the $3\,^2S_{1/2}$ and $3\,^2P_{1/2}$ states of atomic hydrogen in zero magnetic field.

experiment requires a fast hydrogen beam rather than the beams with thermal velocities used in earlier experiments.[10] The natural lifetime of the $3\,^2S_{1/2}$ state is 160 nsec; the natural lifetime of the $3\,^2P_{1/2}$ state is 5.4 nsec.

Figure 1 shows the energy-level diagram for the $3\,^2S_{1/2}$ and $3\,^2P_{1/2}$ states of atomic hydrogen in zero magnetic field. A rf electric field will induce between the states three transitions which overlap strongly and which make a precision determination of the center of the resonance difficult. If, however, the $^2S_{1/2}$, $F=1$ states are removed from the beam without affecting the $^2S_{1/2}$, $F=0$ states, only one allowed transition will connect the two levels. This hyperfine-state selection is accomplished by passing the beam through an rf field at 341 MHz. By mixing preferentially the $^2S_{1/2}$, $F=1$ state with the $^2P_{1/2}$ states and hence reducing the lifetime of the $^2S_{1/2}$, $F=1$ state, this rf field quenches the $^2S_{1/2}$, $F=1$ states without appreciably affecting the $^2S_{1/2}$, $F=0$ states. Two consecutive rf fields with orthogonal polarization are used to ensure quenching of all the m_F levels.

Figure 2 shows the principal components of the apparatus. Protons are extracted from an rf ion source, accelerated by a gap lens to roughly 20 keV, and focused into a parallel beam by an electrostatic lens. This beam is sent through a windowless differentially pumped gas target in which there is nitrogen at a pressure of 5×10^{-3} torr. The protons capture electrons and form excited- or ground-state hydrogen atoms. Subsequently, this beam enters the separated-oscillating-field region (RF11 and RF12) and the hyperfine-state selector (RF2). The hyperfine-state selection is performed after the separated oscillating fields to ensure that cascading effects from higher n states remain unimportant. At the end of the rf-state selector a photomultiplier observes selectively Balmer α photons. At resonance, most S states will be converted

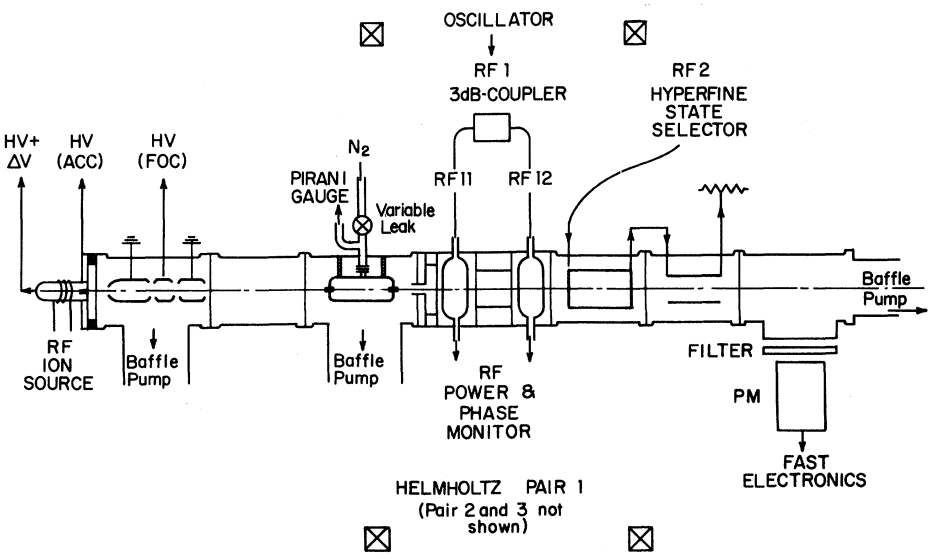

FIG. 2. Schematic diagram of the apparatus.

into P states which decay very rapidly and do not contribute to the photomultiplier signal. Thus the resonance condition is detected as a decrease in count rate. Three orthogonal Helmholtz pairs are used to cancel the earth's magnetic field.

III. THEORY OF THE LINE SHAPE

This treatment follows in its spirit Lamb's original work[10,11] and is a straightforward extension of Ramsey's treatment.[9] The dynamics of the atom-rf-field system is assumed to be described by the Hamiltonian

$$H = H_O + H_D - \vec{\mu}_E \cdot \vec{E}_0 \cos(\omega t + \delta) , \tag{1}$$

where H_O is a Hermitian operator yielding the energy levels

$$H_O|1\rangle = \hbar\omega_1|1\rangle , \quad H_O|2\rangle = \hbar\omega_2|2\rangle ; \tag{2}$$

H_D is a phenomenological anti-Hermitian operator accounting for the decay rates

$$\begin{aligned} H_D|1\rangle &= -\tfrac{1}{2} i\hbar\gamma_1|1\rangle , \\ H_D|2\rangle &= -\tfrac{1}{2} i\hbar\gamma_2|2\rangle ; \end{aligned} \tag{3}$$

$\vec{\mu}_E$ is the electric-dipole-moment operator and $\vec{E}_0 \cos(\omega t + \delta)$ the applied oscillating electric field. The system is described by the wave function

$$|\psi\rangle = c_1(t)|1\rangle + c_2(t)|2\rangle , \tag{4}$$

and the time evolution is given by the time-dependent Schrödinger equation

$$i\hbar \frac{\partial|\psi\rangle}{\partial t} = H|\psi\rangle . \tag{5}$$

The combination of Eqs. (1), (4), and (5) gives

$$i\dot{c}_1 = \omega_1 c_1 - i\tfrac{1}{2}\gamma_1 c_1 + 2Vc_2 \cos(\omega t + \delta) , \tag{6a}$$

$$i\dot{c}_2 = \omega_2 c_2 - i\tfrac{1}{2}\gamma_2 c_2 + 2Vc_1 \cos(\omega t + \delta) , \tag{6b}$$

where $V = -(1/2\hbar)\langle 1|\mu_E E_O|2\rangle$. If we neglect the counter rotating component of the rf field, Eq. (6) becomes

$$i\dot{c}_1 = \omega_1 c_1 - i\tfrac{1}{2}\gamma_1 c_1 + Vc_2 e^{-i(\omega t+\delta)} , \tag{7a}$$

$$i\dot{c}_2 = \omega_2 c_2 - i\tfrac{1}{2}\gamma_2 c_2 + Vc_1 e^{i(\omega t+\delta)} . \tag{7b}$$

For the initial conditions at $t = 0$

$$c_1(t) = c_1(0) , \tag{8a}$$

$$c_2(t) = c_2(0) , \tag{8b}$$

the solutions for Eq. (7) are

$$\begin{aligned} c_1(t) = \exp[&-\tfrac{1}{4}(\gamma_1+\gamma_2)t - i(\tfrac{1}{2})(\omega+\omega_1+\omega_2)t] \\ &\times[(\cos\tfrac{1}{2}at + i\cos\theta\sin\tfrac{1}{2}at)c_1(0) \\ &\quad - e^{-i\delta}(i\sin\theta\sin\tfrac{1}{2}at)c_2(0)] , \end{aligned} \tag{9a}$$

$$\begin{aligned} c_2(t) = \exp[&-\tfrac{1}{4}(\gamma_1+\gamma_2)t + i(\tfrac{1}{2})(\omega-\omega_1-\omega_2)t] \\ &\times[-e^{i\delta}(i\sin\theta\sin\tfrac{1}{2}at)c_1(0) \\ &\quad + (\cos\tfrac{1}{2}at - i\cos\theta\sin\tfrac{1}{2}at)c_2(0)] . \end{aligned} \tag{9b}$$

Here

$$a = [4V^2 + (\Omega + iQ)^2]^{1/2} ; \tag{10}$$

$$\omega_0 = \omega_1 - \omega_2 ; \tag{11}$$

$$\Omega = \omega - \omega_0 ; \tag{12}$$

$$Q = \tfrac{1}{2}(\gamma_1 - \gamma_2) ; \tag{13}$$

$$\sin\theta = 2V/a ; \tag{14}$$

$$\cos\theta = (\Omega + iQ)/a . \tag{15}$$

First we specialize the above results to the conventional single-field rf spectroscopy experiment. At time $t = 0$, the atom is assumed to be in state $|1\rangle$ and to enter the rf field. At the time τ the atom leaves the rf field. At the point the atom leaves the rf field its state is given by

$$\begin{aligned} c_1(\tau) = \exp[&-\tfrac{1}{4}(\gamma_1+\gamma_2)\tau - i(\tfrac{1}{2})(\omega+\omega_1+\omega_2)\tau] \\ &\times(\cos\tfrac{1}{2}a\tau + i\cos\theta\sin\tfrac{1}{2}a\tau) , \end{aligned} \tag{16a}$$

$$\begin{aligned} c_2(\tau) = \exp[&-\tfrac{1}{4}(\gamma_1+\gamma_2)\tau + i(\tfrac{1}{2})(\omega-\omega_1-\omega_2)\tau] \\ &\times(-ie^{i\delta}\sin\theta\sin\tfrac{1}{2}a\tau) . \end{aligned} \tag{16b}$$

Apart from an over-all factor $e^{-(\gamma_1+\gamma_2)\tau/4}$, these expressions depend only on the difference $Q = \frac{1}{2}(\gamma_1 - \gamma_2)$. In the special case where

$$\gamma_1 = \gamma_2 ,$$

the radiative decay of the levels does not change the relative population of the two states and the effect of the rf field is the same as that for two stable levels.

Equation (16) can be used to derive an expression for the rf field strength required to optimize the transition probability so that at resonance all atoms initially in the 1 state make a transition to the 2 state. This information is important for effective operation of the hyperfine-state selector. For rf fields where

$$4V^2 > Q^2 , \tag{17}$$

the occupation probability for the initial state at the exit of the rf field is

$$|c_1(\tau)|^2 = e^{-(\gamma_1+\gamma_2)\tau/2}\,[\cos\tfrac{1}{2}a'\tau - (Q/a')\sin\tfrac{1}{2}a'\tau]^2 ,$$

where

$$a' = (4V^2 - Q^2)^{1/2} .$$

The occupation probability is zero when

$$\tan\tfrac{1}{2}a'\tau = a'/Q . \tag{18}$$

Figure 3 shows the theoretical line profile for a single oscillatory field when the strength of the rf field is kept a constant value. The linewidth only approaches the natural linewidth when the time spent in the rf field is much longer than the lifetime of the P state (5.4 nsec).

We will now specialize to the case of two sepa-

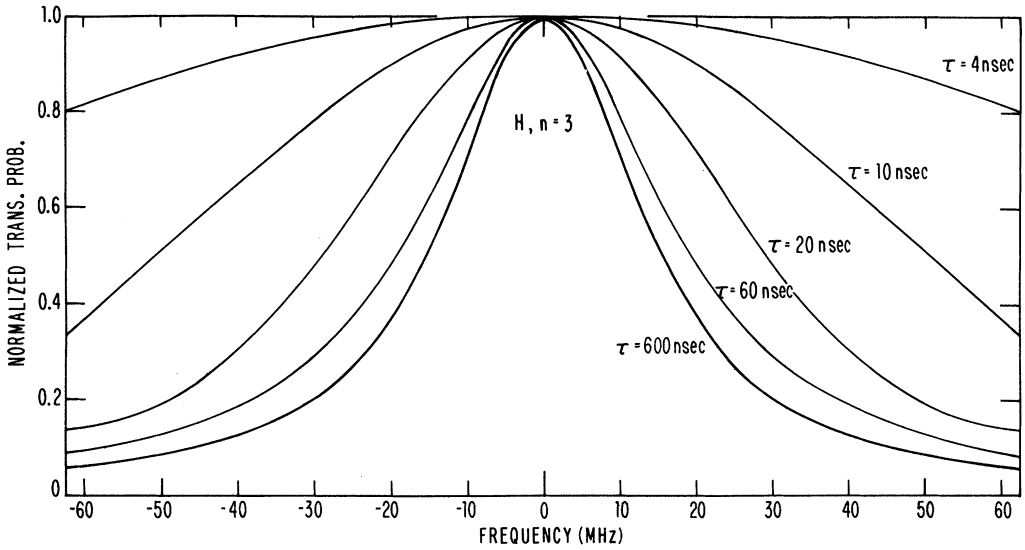

FIG. 3. Plot of the theoretical line profile for a single field of such a length that the atoms spend a time τ in it. The ordinate is proportional to the probability for an atom initially in the S state to take an rf-induced transition from the S to the P state. The curves have been normalized so that they are one at the center of the line. The rf field strength is the same for all the curves.

rated oscillating fields. An atom initially in the pure state 1 enters at time $t=0$ an rf field $\vec{E}_0\cos\omega t$ and at time τ it leaves this field. After spending a time T in a region with no external fields the atom spends a time τ in a field $\vec{E}_0\cos(\omega t+\delta)$. The amplitudes of the wave function at the exit of the second rf field can be calculated by repeated use of Eqs. (9). They are

$$c_1(\tau+T+\tau)=\exp[-\tfrac{1}{2}(\gamma_1+\gamma_2)\,\tau-\tfrac{1}{2}\gamma_1 T-i(\omega+\omega_1+\omega_2)\tau-i\omega_1 T]$$
$$\times\{(\cos\tfrac{1}{2}a\tau+i\cos\theta\sin\tfrac{1}{2}a\tau)^2-\exp[\tfrac{1}{2}(\gamma_1-\gamma_2)T-i(\delta+\Omega T)]\sin^2\theta\sin^2\tfrac{1}{2}a\tau\}, \quad (19a)$$

$$c_2(\tau+T+\tau)=\exp[-\tfrac{1}{2}(\gamma_1+\gamma_2)\tau-\tfrac{1}{2}\gamma_2 T+i(\omega-\omega_1-\omega_2)\tau-i\omega_2 T]$$
$$\times(-i\sin\theta\sin\tfrac{1}{2}a\tau)\{(\cos\tfrac{1}{2}a\tau-i\cos\theta\sin\tfrac{1}{2}a\tau)+\exp[\tfrac{1}{2}(\gamma_2-\gamma_1)T+i(\delta+\Omega T)](\cos\tfrac{1}{2}a\tau+i\cos\theta\sin\tfrac{1}{2}a\tau)\}\,. \quad (19b)$$

The final probability for state 1, which is

$$|c_1(\tau+T+\tau)|^2,$$

contains an interference term of the form

$$\cos(\Omega T+\delta+\Gamma(Q,\ \gamma_1,\ \gamma_2,\ \tau))\,.$$

This is the term which is exploited to select P states that live longer than a mean life and thus to narrow the line. The dependence of the interference term on the rf phase δ can be used to isolate the interference term and to increase the effective signal by a factor of 2. If the signal is taken to be proportional to the difference in probability for an atom to be in state 1 when the phase δ is switched from $\delta=0$ to $\delta=\pi$, we obtain

$$S=|c_1(\tau+T+\tau)|^2_{\delta=\pi}-|c_1(\tau+T+\tau)|^2_{\delta=0}\,, \quad (20)$$

$$S=2\exp[-\tfrac{1}{2}(\gamma_1+\gamma_2)(2\tau+T)]$$
$$\times|\cos\tfrac{1}{2}a\tau+i\cos\theta\sin\tfrac{1}{2}a\tau|^2$$
$$\times|\sin\theta\sin\tfrac{1}{2}a\tau|^2\cos(\Omega T-\Gamma)\,, \quad (21)$$

where

$$\Gamma=2\arg\frac{\sin\theta\sin\tfrac{1}{2}a\tau}{\cos\tfrac{1}{2}a\tau+i\cos\theta\sin\tfrac{1}{2}a\tau}\,. \quad (22)$$

Γ is an odd function of Ω such that $\Gamma=0$ for $\Omega=0$. Figure 4 shows a plot of Eq. (21) for various T and for the parameters relevant to the hydrogen $n=3$, S-P system used in this experiment. In particular

$$\tau=15.5\times10^{-9}/\text{sec}\,,\quad \gamma_1=0.063\times10^8/\text{sec}\,,$$
$$\gamma_2=1.86\times10^8/\text{sec}\,,\quad 2V=1.83\times10^8/\text{sec}\,.$$

These parameters correspond to a value for $2V/Q$ which is somewhat greater than the optimum value determined by the equation

$$\tan\tfrac{1}{2}a'\tau=a'/Q \quad (23)$$

and which exceeds the value used for the final measurements.

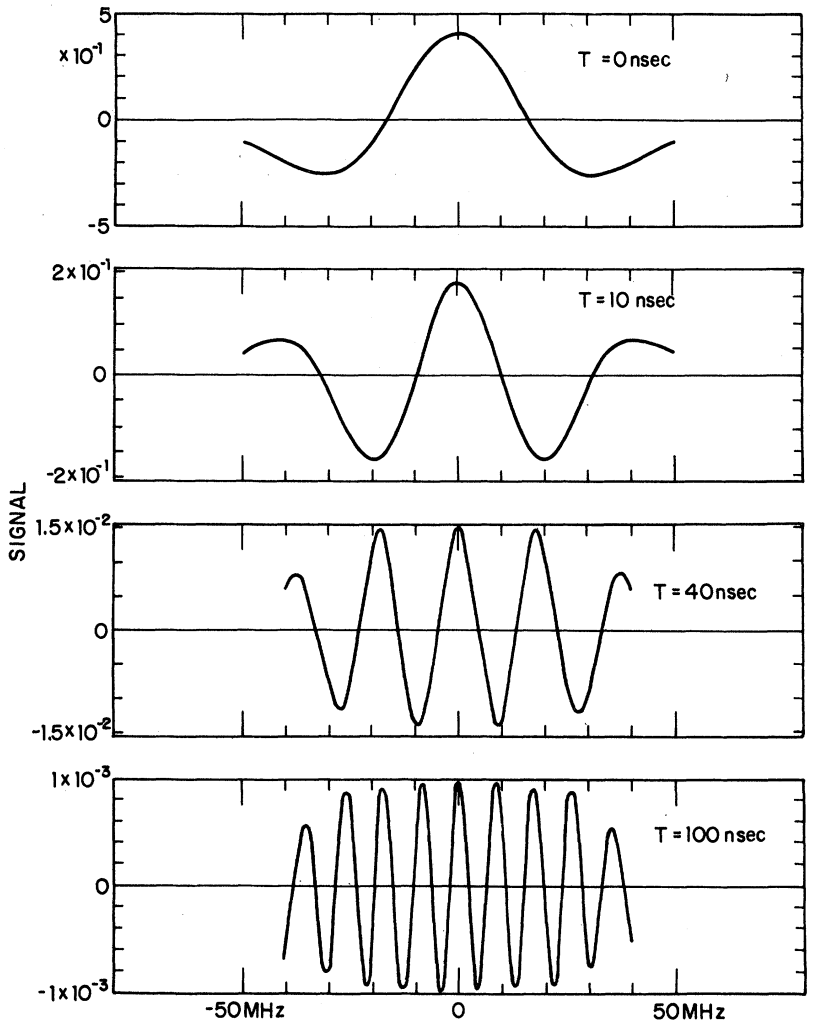

FIG. 4. Plot of the theoretical line profile for the separated oscillating fields. The time required for the atoms to traverse each of the two fields is 15.5 nsec. T gives the time the atoms spend between the two fields. The signal is defined as the difference between the number of S-state atoms reaching the detector when the relative phase of the two rf fields is switched from 0° to 180°.

The use of the separated oscillating fields gives rise to two kinds of line narrowing. The first line narrowing occurs when one replaces a single rf field by two separated oscillating fields with the same over-all length and observes the signal S [Eq. (21)]. This is called interference narrowing and it can be almost as large as a factor of 2. The second source of line narrowing results from the selection of atoms which live longer than a mean P-state lifetime. The linewidth in this case is determined by the time spent between the two rf fields and the narrowing can be characterized as uncertainty-principle narrowing.

IV. APPARATUS

A. Formation of Hydrogen Beam

Figure 5 shows a diagram of the ion source, the focusing lens, and the charge-exchange cell. Protons were produced in a conventional rf ion source which had a 1-mm-diam extraction channel.[12] The rf oscillator was inductively coupled to the glass vessel and delivered up to 50 W of rf power at 90 MHz. Hydrogen gas was bled directly into the glass vessel and the rate was controlled by an adjustable leak. After emerging from the source the protons were accelerated through a gap lens which was formed by the extraction channel at the positive accelerating potential (18–20 kV) and the first electrode of an electrostatic einzel lens which was kept at ground potential. The design parameters for this lens were obtained from the treatment by Ollendorf.[13] The focusing voltage was adjusted to produce a parallel or slightly convergent beam. Measurements of the profile of the focused proton beam showed that roughly 90% of the beam was contained in an area with a 2-mm diameter. After the focusing lens the beam passed through a 12-cm field-free region before reaching the charge-capture target.

In the early work[14] a 10 $\mu g/cm^2$ carbon foil was used as a target.[15] This was an easy and straight-

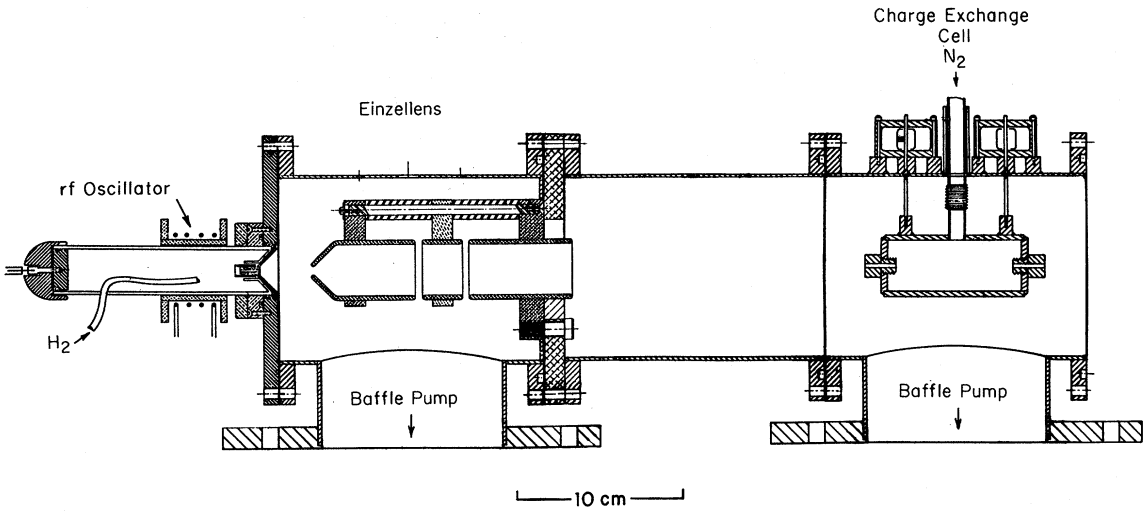

FIG. 5. Diagram of the front end of the accelerator showing the ion source, the focusing lens, and the charge-exchange cell.

forward approach, which had, however, several serious drawbacks. The foil was burned out in minutes using proton currents in excess of 1 μA. To increase the lifetime to several hours, the ion current had to be limited to less than 0.5 μA. Despite this low beam intensity the foil exhibited aging effects and the signal decreased slowly with time. The foil was therefore replaced with a windowless differentially pumped gas target.

From a compilation of charge-capture cross sections[16,17] we estimated that a target thickness of 0.1 torr cm would give a saturation neutralization of 85% for proton energies of 20 keV. With the exception of Cs vapor, this result is almost independent of the nature of the gas for targets with $Z > 7$. For convenience and simplicity we used N_2 as a target gas in all our measurements. As shown in Fig. 5, the target is a 10-cm-long cell with entrance and exit orifices which are 2 cm long and 0.24 cm in diameter. The target could be positioned mechanically under running conditions in order to optimize the alignment. The gas pressure was set by a precision variable leak and monitored with a Pirani gauge. The target pressure was usually kept between 5 and 10×10^{-3} torr. This resulted in a pressure of $(1-2)\times10^{-6}$ torr in the chamber containing the target.

The installation of the gas target proved to be advantageous on several accounts. The beam maintained its high degree of collimation after passage through the target; this increased considerably the signal-to-noise ratio. The signal proved to be extremely stable over many hours and the beam intensity was only limited by saturation effects in the electronics.

B. Vacuum System

The ion source and the gas target contributed two large sources of gas and made it necessary to have high pumping speed. Three 4-in. oil diffusion pumps (700 liter/sec pumping speed) were used to evacuate the system. Since oil films could produce insulating layers which would give rise to experimentally uncontrollable stray electric fields, every known precaution was taken to minimize the back streaming of oil into the beam apparatus. All three pumps were fitted with optically dense baffles cooled thermoelectrically to $-30\,^{\circ}$C or with liquid nitrogen. These pumps were also fitted with Edwards High Vacuum Co. cold caps, which according to the manufacturer reduce the back-streaming rate by a factor of 10. Dow Corning 705 pump oil, which has the lowest back-streaming rate of all commercially available pump oils, was used in the diffusion pumps. The fore pumps were fitted with molecular-sieve traps in order to prevent back streaming of fore pump oil into the main chamber.[18]

C. Radio-Frequency System

Each rf interaction region is built as a parallel plate capacitor which is inserted into a 50-Ω coaxial transmission line that is terminated in 50 Ω. The dimensions of the rf capacitor are small (total length 6 cm) compared to the wavelength at the operating point [λ (271 MHz) = 110.7 cm]. A traveling wave propagates through this transmission line and ideally the rf plates present no discontinuity in impedance over the frequency band of interest. A thermistor was used as a 50-Ω termination and to monitor the rf power at each frequency. In

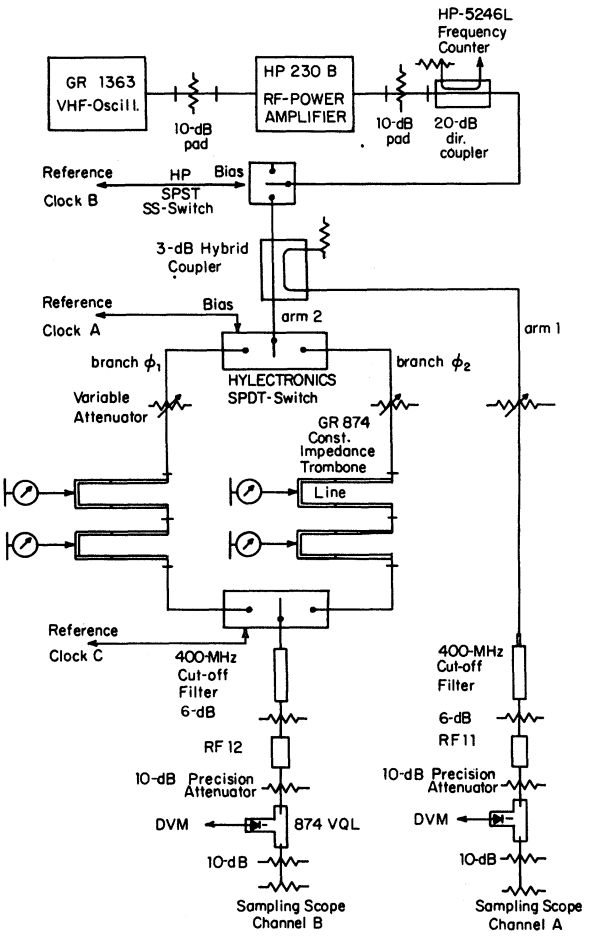

FIG. 6. Schematic diagram of the rf system used to power and monitor the rf cavities.

the two rf spectroscopy chambers the rf travels perpendicular to the hydrogen beam; in the two hyperfine-state selector chambers the rf travels along the direction of the beam.

In the execution of the experiment it is necessary to keep the rf electric field that induces the transitions constant as the frequency is changed. Measurements made of the standing-wave ratio at the entrance and exit ports of the rf chambers showed that there was only a small dependence on frequency over the frequency band of interest.

All the rf-power measurements were made with a Hewlett-Packard model 432A power meter combined with a type 478 thermistor mount. The absolute instrumental accuracy is 0.5%; the accuracy for relative power-level measurements is significantly better. The calibration points of the thermistor, which are traceable to NBS standards, show that the efficiency (power measured/power incident) is a slowly decreasing function of frequency from almost 100% at 10 MHz to 96% at 10 GHz. The smoothness of the frequency response was confirmed by comparing the HP mount with two General Radio model 874 VQL voltmeter (diode) detectors. Within the measurement accuracy of 0.1% all three devices yielded an identical flat frequency response. We therefore concluded that within $\pm 0.1\%$ the thermistor system did not exhibit any frequency dependence across the band of interest.

The apparatus used to drive and monitor the rf spectroscopy chambers is shown in Fig. 6. A General Radio 1363 VHF oscillator with a frequency stability of 1 part in 10^5 after a 24-h warmup period was used as a frequency source. The output was buffered with a 10 dB attenuator, a Hewlett-Packard model 230B amplifier, and another 10 dB attenuator. A Hewlett-Packard model 5303 solid-state single-pole double-throw (SPST) switch gated the rf on and off synchronously with a reference signal. Its output fed a 3-dB hybrid coupler (Merrimac Inc., model PDM-20-30) which divided the rf power with equal phase and amplitude between the two output arms. This coupler is an octave bandwidth device with a center frequency of 300 MHz. The amplitude is balanced to ± 0.2 dB and the phase to $\pm 1°$ over the operating range. The two outputs fed coherently the two rf cavities RF11 and RF12. Arm 1 feeds the rf chamber RF11 through a variable attenuator used for the rf-power fine adjustment and through a 400-MHz cutoff filter, which is inserted to suppress any spurious harmonic content contributed by the oscillator and the solid-state switch. A 6-dB pad ensures further isolation of the rf cavity. The output of the rf chamber is connected directly through a precision 10-dB attenuator to the GR 874 VQL detector, which is terminated in the 50 Ω of the sampling scope input. Arm 2, which feeds the second rf chamber RF12, is arranged in a similar manner. In addition, provision was made to adjust the phase relative to arm 1. Two SPDT solid-state switches (Hylectronics Corp., model S425M) were used to select either branch φ_1 or branch φ_2 synchronously with gating signals provided by the clock A and C outputs. In each branch, two General Radio constant-impedance trombone lines (model 874 LTL) were connected in series providing a total adjustable length of 88 cm each. These trombone lines were coupled to precision vernier calipers, which made precise relative phase changes possible. The phase difference between arm 1 and arm 2 was monitored by a Lissajous figure on the sampling oscilloscope. Since data runs taken for $\Delta\varphi = 0$ and π resulted in a straight line on the scope screen, accurate phase measurements could be made. Using the vernier calipers it was possible to determine the relative trombone settings reliably to ± 1.5 mm; this corresponds to a $\pm 0.5°$ phase uncertainty.

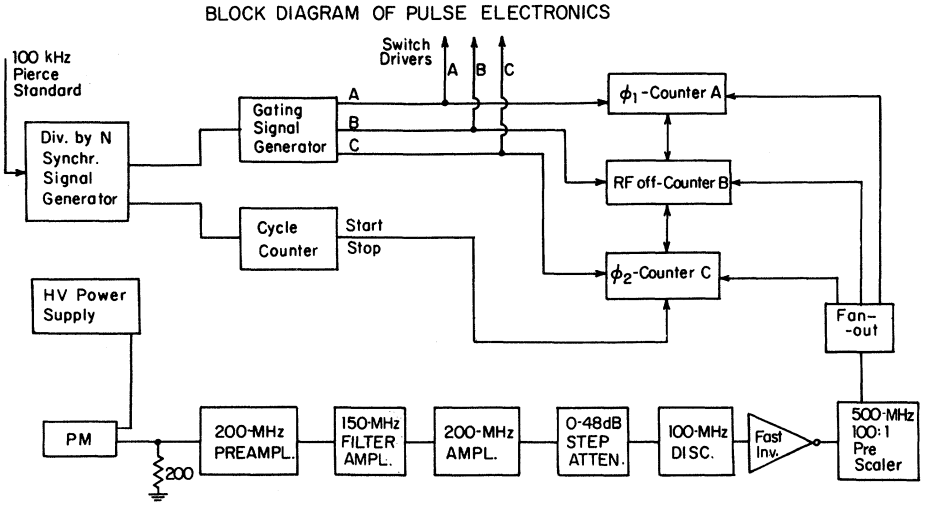

FIG. 7. Block diagram of the electronics used to process the photomultiplier signal.

D. Pulse Electronics

A block diagram of the electronics used to process the photomultiplier signal is shown in Fig. 7. Single-photon counting techniques combined with a digital lock-in detection method were employed. At a set rf frequency, three count rates were recorded by repeating the following measurement cycle. Counter A was gated on when the rf switches were biased to select the rf arms which produced a phase shift $\Delta\varphi_1$ (usually 0°); counter B was gated on when no rf was applied to both chambers; counter C was gated on during the time when the rf-phase difference was $\Delta\varphi_2$ (usually 180°). The reference signal for the timing sequence was provided by a 100-kHz standard signal, stable to 1 part in 10^9, from which time intervals between 1 msec and 1 sec could be synthesized in 1-msec steps. These clock pulses provided the gating signals for the counters and the bias levels for the solid-state switches. The gating times were equalized to better than 1 part in 10^7. A presettable cycle counter provided the start signal and the stop signal after a programmed number of counting sequences.

With the gas target the counting rates were as high as 2 MHz. Care was taken to minimize the dead time by using fast electronics. A "filter amplifier" which was adjusted to provide a high degree of attenuation in a narrow frequency band around 90 MHz was inserted into the amplifying chain. This removed all traces of the rf ion source oscillator from the signal.

V. MEASUREMENTS

The setting for the rf power was determined from an experimental-signal-versus-rf-power-quenching curve. The rf power was set at a level such that the signal was one-half the saturation signal. This required 30–60 mW. This rf-power level is well below the "optimum" level [Eqs. (18) and (23)]; the optimum level would considerably broaden the resonance line.

Panoramic line scans were made by counting at a series of frequencies for a preset time. Points were taken alternately on opposite sides of the line to reduce any drift in the data. Figure 8 shows the line shape for the case where the hyperfine-state selector was not used. The observed line shows the three allowed transitions indicated in the level diagram given in Fig. 1. Figure 8 also shows a least-squares fit to three Lorentzians. In this fit the amplitudes and half-widths of each line and the frequency of one of the lines were allowed to vary. The relative spacing of the lines, which is determined by the hyperfine splitting, was kept fixed.

A series of measurements was made with the two spectroscopy chambers operated in the single-field mode and with the hyperfine-state selector adjusted to remove the $^2S_{1/2}$, $F=1$ states. The geometrical separation between the two chambers was 2 mm; this corresponded to a field-free time $T=1\times10^{-9}$ sec. The relative phase of the two rf fields was kept constant at $\delta=0$. Other relevant parameters are summarized in Table I. These parameters were the same for all the measurements reported here unless otherwise noted.

Figure 9(a) shows a line scan taken with this configuration of the apparatus. It also shows the theoretical line shape calculated using Eq. (17a) and the experimental parameters listed in Table I. The amplitude and the center of the line were adjusted to obtain the best fit between the points at half-maximum. The statistical error in the experimental points is smaller than the size of the dots. Figure 9(b) shows on an expanded scale the difference between the experimental points and the theoretical curve. Between the points at half-maximum, the agreement between the theoretical

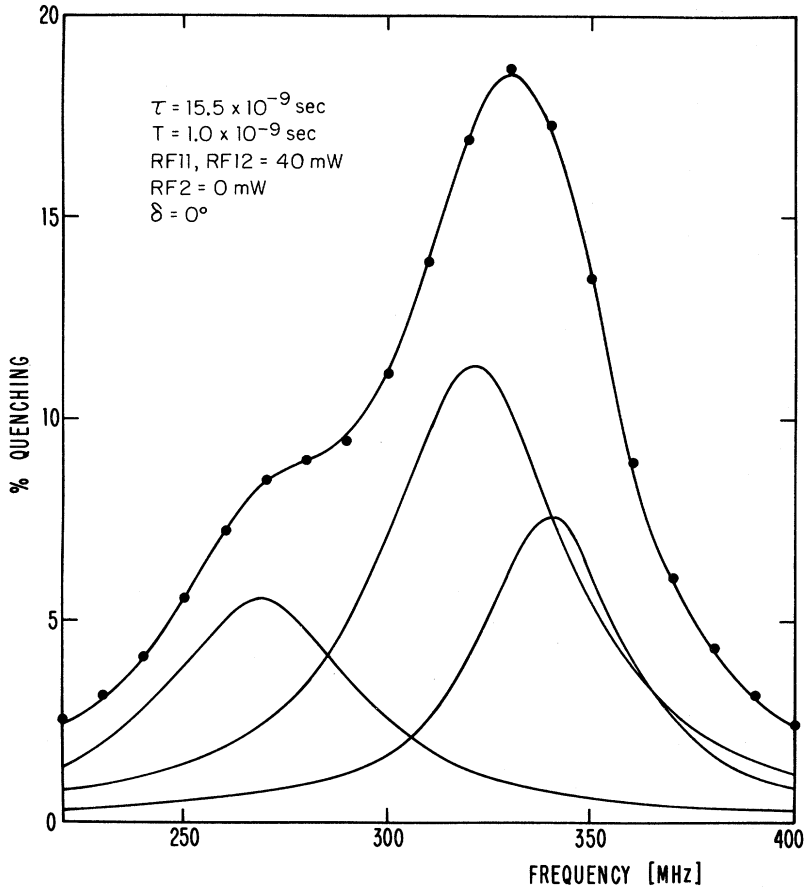

FIG. 8. Line profile for the SF configuration when the hyperfine-state selector is not used. The curves are a fit to three Lorentzian components. For this fit the amplitudes of each line, the half-widths of each line, and the frequency of one of the lines were allowed to vary. The relative spacing of the lines, which is determined by the hyperfine splitting, was kept fixed.

and experimental line shapes is excellent. A change of the experimental input parameter τ by 0.1 nsec would considerably deteriorate the agreement.

There is a significant difference between the theoretical and experimental curves around 330 MHz, which is the center of gravity for the two $^2S_{1/2}$, $F=1 \rightarrow {}^2P_{1/2}$, $F=1$ and $^2P_{1/2}$, $F=0$ transitions. This difference indicates the degree of quenching of the $^2S_{1/2}$, $F=1$ state. On the low-frequency side at 228 MHz, there are traces of the $4D_{5/2} \rightarrow 4F_{7/2}$ transition.[19]

Data for a precision measurement of the center of the resonance were taken by the symmetric-pair method. Starting with the 253-289-MHz pair, which is roughly the points at which the signal is half its maximum value, measurements were made at 2-MHz intervals up to the 269-273-MHz pair. Neighboring points were used to obtain a value of the slope of the resonance to correct for any difference in signal amplitude. The nine measurements of the center constituted a run. The results were averaged to obtain one value for the line center. The error was taken to be the standard deviation of the nine measurements. To eliminate any systematic error due to the first-order Doppler shift, data were taken with the rf wave traveling in opposite directions. 12 runs were made with the rf running from bottom to top and eight runs with the rf running from top to bottom. Table II summarizes the results for these 20 runs.

With the experimental conditions the same as in the single-field measurements, a set of runs was made with the phase δ switched between 0 and π so as to isolate the two-field interference term. Figure 10 shows the experimental line profile and the theoretical line profile calculated using Eqs. (20)

TABLE I. The accelerator and rf settings for the measurements of the $3\,^2S_{1/2}$, $F=0 \rightarrow 3\,^2S_{1/2}$, $F=1$ Lamb-shift transition.

Beam energy	19.5 keV
Beam velocity	$(1.93 \pm 0.01) \times 10^8$ cm sec^{-1}
Length of RF11, RF12	3.0 cm
Time τ in RF11, RF12	15.5×10^{-9} sec
Length of field-free region	0.2 cm
Time T in field-free region	1.0×10^{-9} sec
rf power in RF11, RF12	40.0 mW
rf amplitude in RF11, RF12	$4.00 V_{pp}$/cm
rf amplitude in hyperfine-state selector	$9.50 V_{pp}$/cm
Frequency in hyperfine-state selector	343.0 MHz

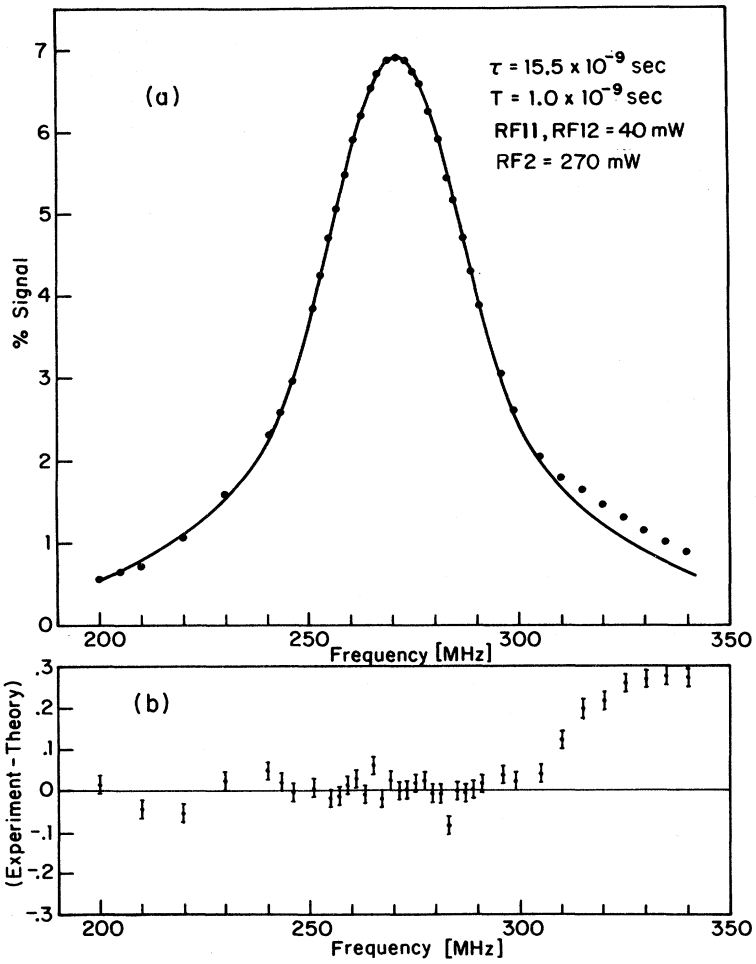

FIG. 9. (a) Line profile for the $3\,^2S_{1/2}$, $F=0 \rightarrow 3\,^2P_{1/2}$, $F=1$ transition with the single-rf-field configuration. The dots show the experimental points. The statistical errors on the experimental points are smaller than the dots. The curve is the theoretical line shape calculated using the parameters shown in the figure and in Eq. 7(a). (b) The difference between theory and experiment for the data and the theoretical curve given in part (a).

and (22). The only adjustable parameter was the height of the signal at resonance. The discrepancy between the experimental and theoretical lines between 230 and 240 MHz may be due to the $4\,^2D_{5/2} - 4\,^2F_{7/2}$ contamination at 228 MHz. The discrepancy between 300 and 320 MHz, however, can only be explained with difficulty as due to the contribution from the $^2S_{1/2}$, $F=1$ state. The possibility of an error in the phase measurement was carefully checked and can be excluded. The two oscillating fields gave a full width at half-maximum of 30 MHz. This can be compared with the width of 44 MHz obtained with the single-oscillating-field mode.

Data for a precision measurement of the center with the separated oscillating fields were taken in the same manner as with the single field. Table III summarizes these measurements.

Measurements were also made with the two oscillating fields separated by 3.6 cm. This corresponds to a field-free time $T=18$ nsec. Figure 11 shows the experimental and theoretical line profiles for this configuration. The observed linewidth is $\frac{4}{10}$ of the single-field linewidth and $\frac{2}{3}$ of the natural linewidth for this transition. The side peaks are particularly prominent and can be used to estimate the influence of various parameters which can distort the symmetry of the line. Due to the difficulty of obtaining resonance lines in the $n=3$ level free of distortions due to neighboring lines, we did not include observations with these extremely narrowed lines in the determination of the Lamb shift.

VI. DETERMINATION OF THE LAMB SHIFT

In order to determine the Lamb shift from the measurements, it is necessary to make several corrections. This section describes in detail the corrections and gives the final result for the Lamb shift. The corrections are summarized in Tables II–V.

A. Radio-Frequency Stark Shift

Since a linearly polarized rf field was used to drive the transitions, there is a shift in the center of the resonance due to the antiresonant component of the rf field. In the magnetic-resonance literature, this shift is called the Bloch-Siegert effect.[20]

TABLE II. Summary of the measurements for the single-field data runs and the results obtained after the correction for the rf Stark effect. The errors are one standard deviation.

rf direction	rf power (mW)	Measured center frequency (MHz)	Corrected center frequency (MHz)
	30	271.1935 ± 0.1448	271.1121 ± 0.1448
	30	271.3205 ± 0.1508	271.2391 ± 0.1508
	30	271.2233 ± 0.1568	271.1419 ± 0.1568
	30	271.0347 ± 0.2875	270.9533 ± 0.2875
Bottom	30	270.9398 ± 0.1816	270.8584 ± 0.1816
to	40	271.0175 ± 0.3387	270.9235 ± 0.3387
top	40	271.4192 ± 0.2595	271.3252 ± 0.2595
	40	270.9723 ± 0.2118	270.8783 ± 0.2118
	50	271.1296 ± 0.7038	271.0245 ± 0.7038
	50	271.4996 ± 0.4920	271.3945 ± 0.4920
	50	271.1758 ± 0.3169	271.0707 ± 0.3169
	50	271.1477 ± 0.2009	271.0426 ± 0.2009
Weighted average (rf bottom → top)			271.0828 ± 0.0618
	30	271.0782 ± 0.1481	270.9968 ± 0.1481
	30	271.1125 ± 0.1289	271.0311 ± 0.1289
Top	30	271.0629 ± 0.3494	270.9815 ± 0.3494
to	30	271.0949 ± 0.3747	271.0135 ± 0.3747
bottom	30	271.0968 ± 0.2262	271.0154 ± 0.2262
	30	271.1690 ± 0.2656	271.0876 ± 0.2656
	30	271.1342 ± 0.1684	271.0528 ± 0.1684
	30	271.1863 ± 0.1016	271.1049 ± 0.1016
Weighted average (rf top → bottom)			271.1051 ± 0.0590
Average interval			271.0940 ± 0.0427

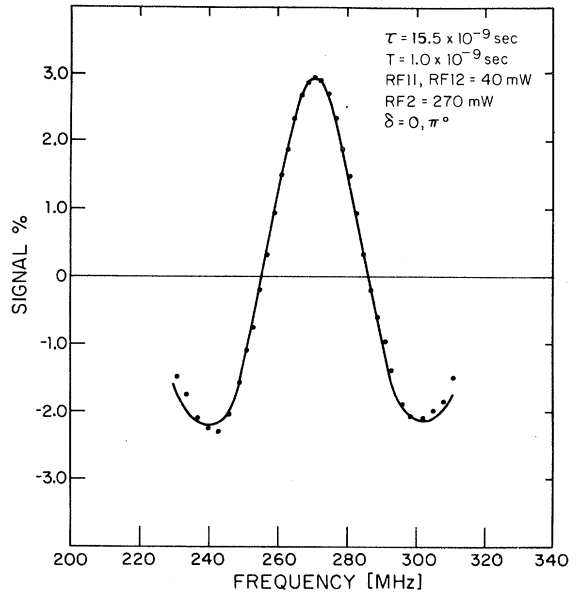

FIG. 10. Line profile for the $3\,^2S_{1/2}$, $F=0 \rightarrow 3\,^2P_{1/2}$, $F=1$ transition with the separated-oscillating-field configuration. The statistical errors on the experimental points are smaller than the dots. The curve is the theoretical line shape.

This effect has been studies for both single-oscillating-field[20, 21] and separated-oscillating-field measurements[22] for the case when the levels are stable. Lamb has given an approximate analysis of the problem for unstable levels.[11]

An approximate solution of Eqs. 6(a) and 6(b) taking into account the counter rotating component of the rf field shows that for a single oscillating field the resonance frequency is increased by the quantity

$$\Delta\omega = [4V^2/(Q^2 + 4\omega_0^2)]\,\omega_0 . \qquad (24)$$

For $Q = 0$ this expression agrees with that given by Bloch and Siegert. However, when $Q \neq 0$, it does not agree with the expression given by Lamb.

For the general case of separated oscillating fields the resonance is displaced less than the amount expected due to the oscillating field. The reduction depends on the ratio τ/T. For the relevant measurements made in this experiment there was a very small separation between the two fields and the Bloch-Siegert displacement is the same as that for a single oscillating field.

Since the data were taken with more than one value for the rf field, the data were first corrected for the displacement due to the antiresonant com-

TABLE III. Summary of the measurements for separated-oscillating-field data runs and the results obtained after the correction for the rf Stark effect. The errors are one standard deviation.

rf direction	rf power (mW)	Measured center frequency (MHz)	Calculated center frequency (MHz)
	30	270.9562 ± 0.1113	270.8748 ± 0.1113
	30	271.0903 ± 0.1840	271.0089 ± 0.1840
	30	271.1353 ± 0.0604	271.0539 ± 0.0604
	30	271.2030 ± 0.1535	271.1216 ± 0.1535
Bottom	30	271.0252 ± 0.1577	270.9438 ± 0.1577
to	40	271.0656 ± 0.1072	270.9716 ± 0.1072
top	40	270.9587 ± 0.2318	270.8647 ± 0.2318
	50	271.0427 ± 0.1208	270.9376 ± 0.1208
	50	270.8746 ± 0.1881	270.7695 ± 0.1881
	50	270.9232 ± 0.1980	270.8181 ± 0.1980
	50	270.7734 ± 0.2052	270.6683 ± 0.2052
Weighted average (rf bottom → top)			270.9715 ± 0.0373
	30	270.9686 ± 0.2078	270.8872 ± 0.2078
	30	271.1699 ± 0.1296	271.0885 ± 0.1296
	30	270.9844 ± 0.2494	271.9030 ± 0.2494
Top	30	271.0801 ± 0.1563	270.9987 ± 0.1563
to	30	270.9593 ± 0.1009	270.8779 ± 0.1009
bottom	30	271.1095 ± 0.1739	271.0281 ± 0.1739
	30	270.9222 ± 0.1332	270.8408 ± 0.1332
	30	271.1639 ± 0.1427	271.0825 ± 0.1427
Weighted average (rf top → bottom)			270.9577 ± 0.0515
Average interval			270.9646 ± 0.0318

TABLE IV. Summary of the correction to the line centers due to neighboring transitions. All units are MHz.

	Single-field data	Separated-field data
Raw center	271.0940 ± 0.0427	270.9646 ± 0.0318
Δ(330)	−0.0894 ± 0.0190	+0.0292 ± 0.0065
Δ(228)	+0.0349 ± 0.0175	−0.0212 ± 0.0106
Corrected center	271.0395 ± 0.0499	270.9726 ± 0.0341

ponent of the rf field. Table II summarizes the corrections for the single-oscillating-field measurement; Table III summarizes the corrections for the separated-oscillating-field measurements. These tables also give the average values for the $3\,^2S_{1/2}$, $F=0\rightarrow 3\,^2P_{1/2}$, $F=1$ splitting. The uncertainty in the rf Stark shift was taken to be ±0.0136 MHz; this is one-third of the correction at 30-mW rf power. This uncertainty was not included until the summary in Table V.

B. Correction for Overlapping Lines

The distortion of the resonance by the two neighboring transitions is the most serious source of systematic error in the experiment. The $3\,^2S_{1/2}$, $F=1\rightarrow 3\,^2S_{1/2}$, $F=0$ transition at 341 MHz and the $3\,^2S_{1/2}$, $F=1\rightarrow 3\,^2P_{1/2}$, $F=1$ transition at 323 MHz were analyzed as a single transition at 330 MHz and found to contribute (0.31 ± 0.06)% to the signal at 330 MHz. This model was then used to calculate the shift in the center of the $3\,^2S_{1/2}$, $F=0\rightarrow 3\,^2P_{1/2}$, $F=1$ transition. For the single-rf-field measurement

$$\Delta(\mathrm{SF},\ 330) = -(0.0894 \pm 0.0190)\ \mathrm{MHz}\ . \qquad (25)$$

For the separated-oscillatory-field measurement

$$\Delta(\mathrm{SepF},\ 330) = +(0.0292 \pm 0.0065)\ \mathrm{MHz}\ . \qquad (26)$$

A similar procedure was used with the 228-MHz contamination. The 228-MHz resonance was found to contribute (0.1 ± 0.05)% to the signal at 228 MHz and to give for the shift in the center of the $3\,^2S_{1/2}$, $F=0\rightarrow 3\,^2P_{1/2}$, $F=1$ transition

$$\Delta(\mathrm{SF},\ 228) = +(0.0349 \pm 0.0175)\ \mathrm{MHz}\ , \qquad (27)$$

$$\Delta(\mathrm{SepF},\ 228) = -(0.0212 \pm 0.0106)\ \mathrm{MHz}\ . \qquad (28)$$

Table IV summarizes these corrections and shows that the overlap correction considerably reduces the discrepancy between the single-field and separated-field data. The over-all error due to incomplete knowledge of the line shape was taken to be 0.0212 MHz.

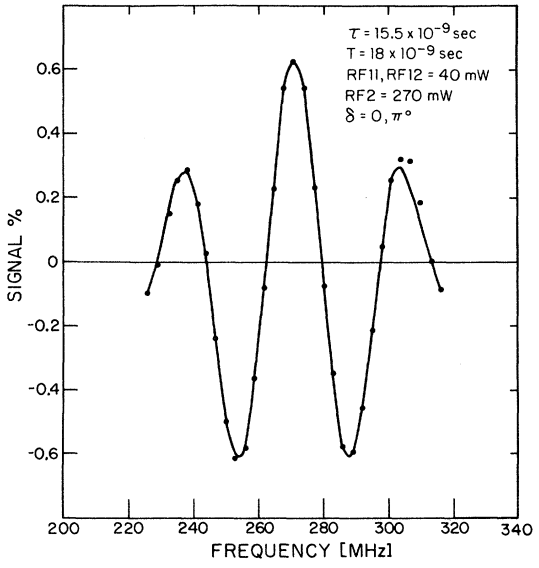

FIG. 11. Line profile for the $3\,^2S_{1/2}$, $F=0\rightarrow 3\,^2P_{1/2}$, $F=1$ transition with the separated-oscillating-field configuration such that the field-free time is 18 nsec. The statistical errors on the experimental points are smaller than the dots. The curve is the theoretical line shape.

C. Stark Effect

In order to minimize stray electric fields, all the surfaces seen by the beam were carefully cleaned to remove all traces of oil and care was taken to prevent the accumulation of oil films inside the apparatus during the course of the experiment. The two data sets with the rf propagating in different directions were taken approximately 1 week apart. During this time the apparatus was not opened and cleaned. The difference of the average SF and SepF measurements for these two data sets was taken as a one-standard-deviation estimate of the uncertainty due to stray electric fields. This gives

TABLE V. Summary of the experimental results, corrections, and error analysis. All errors are one standard deviation.

	Results (MHz)
Single field	271.0395 ± 0.0499
Separated field	270.9726 ± 0.0341
Direct average	271.0061 ± 0.0302
Line distortion	0.0000 ± 0.0212
Stark effect (electrostatic)	0.0000 ± 0.0043
Space charge	−0.0357 ± 0.0258
Uncertainty in rf Stark	0.0000 ± 0.0136
Time dilation	+0.0056 ± 0.0000
rf-power correction	+0.0030 ± 0.0030
rf-phase correction	0.0000 ± 0.0100
$^3S_{1/2}$, $F=0\rightarrow {}^3P_{1/2}$, $F=1$	270.9790 ± 0.0484
Hyperfine correction ($S_{1/2}$)	+39.4583 ± 0.0009
Hyperfine correction ($P_{1/2}$)	+4.3817 ± 0.0001
δ(H, $n=3$, expt)	314.819 ± 0.048

$$\Delta(\text{stray fields}) = (0.000 \pm 0.0043)\ \text{MHz} . \quad (29)$$

D. Space-Charge Effects

Most of the measurements were made with a proton current of 20 μA and 50% neutralization in the gas target. To correct for shifts due to the electric fields produced by the protons in the beam, measurements were made with the beam current alternating between 20 and 8 μA. An extrapolation to zero beam current gave for measurements made at 20 μA the correction

$$\Delta(\text{space charge}) = -(0.0357 \pm 0.0258)\ \text{MHz} . \quad (30)$$

E. Deuterium Contamination

Commercial hydrogen gas which contained deuterium in the ratio of the natural abundances

$$D/H = 1.5 \times 10^{-4}$$

was used in the ion source. This ratio is sufficiently small that the distortion of the lines due to deuterium resonances is negligible.

F. Residual Magnetic Field

The residual magnetic field could shift the line through the Zeeman effect and Stark shifts due to motional electric fields. Since the residual magnetic field was less than 10 mG both effects contribute much less than 1 kHz.

G. Doppler Shift

The rf plates were designed so that the traveling rf field was perpendicular to the direction of the beam. Thus there should be no first-order Doppler shift. To cancel out any first-order Doppler shift due to misalignment of the rf field, data were taken with the rf traveling in both directions and averaged to obtain the final splitting.

The equation

$$\nu(\text{lab}) = \nu(\text{atom})(1 - \beta^2)^{1/2} , \quad (31)$$

where β is the velocity of the atom divided by the velocity of light, was used to correct for the second-order Doppler effect. This correction is sometimes known as time dilation. For this experiment

$$\Delta(\text{T. D.}) = +(0.0056 \pm 0.000)\ \text{MHz} . \quad (32)$$

H. rf-Power Variation

With fixed rf power the electric field which induces the transitions varied slightly over the frequency band of interest. The correction for this variation in rf response was measured to be

$$\Delta(\text{rf response}) = +(0.0030 \pm 0.0030)\ \text{MHz} . \quad (33)$$

The error in this correction indicates the difficulty of measuring precisely the correction at this very low level of nonuniform rf response.

I. rf-Phase Error

It is estimated that the relative phase between the two rf chambers was measured with an accuracy of $\pm 0.5°$. Since the phase had to be measured and readjusted every time a different point on the resonance was measured, any adjustment errors were random and averaged to zero.

To make an allowance for any phase misalignment of the oscilloscope channels, we note that a phase error of $\pm 0.5°$ will shift the line center by ± 0.0300 MHz. This can be regarded as a limit of error, and we obtain

$$\Delta(\text{phase}) = (0.0000 \pm 0.0100)\ \text{MHz} \quad (34)$$

as a one-standard-deviation estimate of the phase error.

J. Frequency Error

The time base of the frequency counter was calibrated against laboratory standards which are known to better than 1 in 10^8. As a result there is no uncertainty due to the frequency measurement.

K. Correction for Hyperfine Structure

Since this experiment measured the $3\,^2S_{1/2}$, $F = 0 \rightarrow 3\,^2P_{1/2}$, $F = 1$ transition, it is necessary to know the hyperfine structure of the two levels to extract a value for the Lamb shift. Since no work has been done on the hyperfine structure of the $n = 3$ state of hydrogen, we used as a guide the work by Mittleman[23] on the $n = 1$ and $n = 2$ states. One expects

$$R_{1,n} = \frac{\Delta\nu(n\,^2S_{1/2},\ \text{H})}{\Delta\nu(1\,^2S_{1/2},\ \text{H})} = \frac{1}{n^3}\left[1 + (C_n - C_1)\alpha^3 + (B_n - B_1)\alpha^3 + \cdots\right] . \quad (35)$$

According to Mittleman,

$$C_1 = \tfrac{3}{2} , \quad C_2 = \tfrac{17}{8} , \quad B_2 - B_1 = 5.28 . \quad (36)$$

We shall take

$$C_3 = \tfrac{22}{8} \pm \tfrac{3}{8} \quad (37)$$

and

$$B_3 - B_1 = 0 . \quad (38)$$

Using these constants and[5,24]

$$\Delta\nu(1\,^2S_{1/2},\ \text{H}) = 1420\,405\,752\ \text{Hz} , \quad (39)$$

$$\alpha^{-1} = 137.03602 \pm 0.00021 , \quad (40)$$

we obtain

$$\Delta\nu(3\,^2S_{1/2},\ \text{H}) = (52.6111 \pm 0.0011)\ \text{MHz} . \quad (41)$$

Using this result, the energy levels for the $3\,^2S_{1/2}$ complex can be determined. The hyperfine splitting of the $3\,^2P_{1/2}$ state can be calculated from the work

of Brodsky and Parsons.[25] The results of these calculations are summarized in Fig. 1. Expressed in terms of the corrections required to obtain the Lamb shift from the measured $3\,^2S_{1/2}$, $F=0 \rightarrow 3\,^2P_{1/2}$, $F=1$ transition, the hyperfine splittings are

$$\Delta(3\,^2S_{1/2},\ F=0,\ \mathrm{H}) = +(39.4583 \pm 0.0009)\ \mathrm{MHz}\ , \tag{42}$$

$$\Delta(3\,^2P_{1/2},\ F=1,\ \mathrm{H}) = +(4.3817 \pm 0.0001)\ \mathrm{MHz}\ . \tag{43}$$

After all the corrections are made, we obtain for the Lamb shift

$$\$\,(\mathrm{H},\ n=3,\ \mathrm{expt}) = 314.819 \pm 0.048\ . \tag{44}$$

The measurements and the corrections are summarized in Table V. This value differs slightly from the previously reported value[26] (314.810 ± 0.052) due to certain refinements in the analysis. The most recent theoretical value for the Lamb shift in the $n=3$ state of hydrogen is that given by Erickson,[2]

$$\$\,(\mathrm{H},\ n=3,\ \mathrm{theoret}) = 314.8977 \pm 0.0034\ . \tag{45}$$

This is based on the following values for the fundamental constants:

$$\alpha^{-1} = 137.036020 \pm 0.00021\ , \tag{46a}$$

$$c = 299792.50\ \mathrm{km/sec}\ , \tag{46b}$$

$$\mathcal{R}_\infty = 109737.312\ (\mathrm{cm})^{-1}\ , \tag{46c}$$

$$2e/h = 483.593718\ \mathrm{MHz}/\mu\mathrm{V}, \tag{46d}$$

$$\text{rms nuclear radius} = 0.800 \times 10^{-3}\ \mathrm{cm}\ , \tag{46e}$$

$$\text{proton mass} = 1.007277\ \mathrm{amu}\ , \tag{46f}$$

$$\text{electron mass} = \mathrm{amu}/1822.8449\ . \tag{46g}$$

Table VI summarizes all the measurements of the Lamb shift in the $n=3$ state of hydrogen. The agreement between this measurement and earlier measurements is excellent. The agreement between this measurement and theory is satisfactory. This table shows that the fast-beam separated-oscillating-field method has made possible a significant increase in the experimental precision.

TABLE VI. Summary of the measured values and the theoretical value for the Lamb shift in the $n=3$ state of hydrogen. The experiment of Lamb and Wilcox actually used deuterium; the results have been corrected so as to obtain an equivalent value for hydrogen. All the errors are one standard deviation.

Observer	Method	Result (MHz)	Reference
Lamb and Wilcox	Bottle	314.93 ± 0.40	27
Kleinpoppen	Atomic beam	313.6 ± 2.9	28
Fabjan and Pipkin	Beam foil	315.11 ± 0.89	14
Fabjan and Pipkin	Sep. Osc. Fields	314.819 ± 0.048	This expt
Erickson	Theory	314.898 ± 0.003	2

VII. CONCLUSIONS

A fast-atom-beam technique has been used to obtain a new measurement of the Lamb shift in the $n=3$ state of hydrogen. The use of a fast beam makes it possible to study short-lived states with the inherent advantages of the atomic-beam method and to significantly increase the precision with which the $n=3$ Lamb shift is known. The high signal level and the excellent signal-to-noise ratio indicate that the lines can be further narrowed and the precision increased by another order of magnitude. The measurements also indicate that this technique can be applied to the experimentally more favorable case of the $n=2$ state in hydrogen. This would make possible more precise measurements of both the Lamb shift and the fine-structure interval. The directness of the experimental approach suggests that the increase in precision can be matched with a corresponding improvement in accuracy.

ACKNOWLEDGMENTS

Throughout the course of this experiment we have benefited from numerous discussions with Dr. R. A. Brown. We are also appreciative of his collaboration in the early stages of this work. We were benefited by the assistance of J. Apt and M. P. Silverman at various stages of the experiment. We would like to acknowledge the advice and support of the Jefferson Glass and Machine Shops.

†Research supported in part by the National Science Foundation under Grant No. GP-22787.

*Present address: CERN, Geneva, Switzerland.

[1]For general reviews of the status of quantum electrodynamics see (a) S. J. Brodsky and S. D. Drell, Ann. Rev. Nucl. Sci. 20, 147 (1970); (b) F. M. Pipkin, in *Essays in Physics*, edited by G. K. T. Conn and G. N. Fowler (Academic, London, 1970), p. 1; (c) S. J. Brodsky, 1971 *International Symposium on Electron and Photon Interactions at High Energy* (Laboratory of Nuclear Studies, Cornell University, Ithaca, N.Y., 1972); (d) E. de Rafael, B. Lautrup, and A. Peterman, Phys. Rept. (to be published).

[2]G. W. Erickson, Phys. Rev. Letters 27, 780 (1971).

[3]T. Appelquist and S. J. Brodsky, Phys. Rev. A 2, 2293 (1970).

[4]S. Triebwasser, E. S. Dayhoff, and W. E. Lamb, Jr., Phys. Rev. 89, 98 (1953).

[5]For a critical review of the older measurements see B. N. Taylor, W. H. Parker, and D. N. Langenberg, Rev. Mod. Phys. 41, 375 (1969).

[6]R. T. Robiscoe and T. W. Shyn, Phys. Rev. Letters 24, 559 (1970).

[7]V. W. Hughes, in *Quantum Electronics*, edited by C. H. Townes (Columbia U. P., New York, 1960), p. 582.

[8]According to J. Heberle this technique was also suggested by R. H. Dicke.

[9]N. F. Ramsey, *Molecular Beams* (Oxford U. P., Lon-

don, 1956), p. 124.
[10]W. E. Lamb, Jr. and R. C. Retherford, Phys. Rev. 72, 241 (1947); 79, 549 (1950); 81, 222 (1951); 86, 1014 (1952).
[11]W. E. Lamb, Jr., Phys. Rev. 85, 259 (1952).
[12]C. D. Moak, H. Reese, Jr.,and W. M. Good, Nucleonics 9, 18 (1951).
[13]F. Ollendorff, *Elektronik des Einzelelektrons* (Springer-Verlag, Vienna, 1955).
[14]C. W. Fabjan and F. M. Pipkin, Phys. Rev. Letters 25, 421 (1970).
[15]S. Bashkin, Nucl. Instr. Methods 28, 88 (1964).
[16] S. K. Allison, Rev. Mod. Phys. 30, 1137 (1958).
[17]R. H. Hughes, B. M. Doughty, and A. R. Filippelli, Phys. Rev. 173, 172 (1968).
[18]M. A. Baker and G. H. Staniforth, Vacuum 18, 17 (1968).
[19]C. W. Fabjan, F. M. Pipkin, and M. P. Silverman, Phys. Rev. Letters 26, 347 (1971).
[20]F. Bloch and A. Siegert, Phys. Rev. 57, 522 (1940).
[21]A. F. Stevenson, Phys. Rev. 58, 1061 (1940).
[22]J. H. Shirley, J. Appl. Phys. 34, 783 (1963).
[23]M. H. Mittleman, Phys. Rev. 107, 1170 (1957).
[24]R. Vessot, H. Peters, J. Vanier, T. Beehler, D. Halford, R. Harrach, D. Allan, D. Glaze, C. Snider, J. Barnes, L. Cutler, and L. Bodily, IEEE Trans. Instr. Measur. IM-15, 165 (1966).
[25]S. J. Brodsky and R. G. Parsons, Phys. Rev. 163, 134 (1967).
[26]C. W. Fabjan and F. M. Pipkin, Phys. Letters 36A, 69 (1971).
[27]L. R. Wilcox and W. E. Lamb, Jr., Phys. Rev. 119, 1915 (1960).
[28]H. Kleinpoppen, Z. Physik 164, 174 (1961).

PHYSICAL REVIEW A VOLUME 6, NUMBER 2 AUGUST 1972

Observability of Hyperfine Structure and Lamb, Nuclear-Volume Shifts in $1snl$-$1snl'$ Transitions of Heliumlike Ions

Sidney O. Kastner
Solar Plasmas Branch, Laboratory for Solar Physics, NASA-Goddard Space Flight Center, Greenbelt, Maryland 20771
(Received 29 October 1971; revised manuscript received 13 March 1972)

The hyperfine-structure widths of $1snl$–$1snl'$ transitions in heliumlike ions are estimated for $n=2,3$ and Z up to 30. Relevant parameters such as spin-orbit and electrostatic parameters are also calculated on the basis of screened hydrogenic functions. It is found that the hyperfine-structure widths are greater than 10 Å at accessible visible wavelengths in some cases. Also, absolute wavelength shifts due to Lamb and nuclear-volume effects are of the order of several angstroms.

Herzberg and Moore,[1] in studying magnetic hyperfine structure in the $1s2s$-$1s2p$ transitions of Li II, noted that it was comparable with the fine structure in some cases and could even be larger than the singlet-triplet intervals for large n and l. Such conditions present interesting varieties of coupling schemes. The observed wavelengths of these transitions are also of interest in ascertaining values of Lamb shift and volume-isotope (nuclear electric monopole) shift. The purpose of this article is to explore the importance of nuclear effects in the spectra of the most abundant isotopes of heliumlike ions up to Zn XXIX ($Z\approx30$). As Z increases, the electrons are pulled closer to the nucleus so that nucleus-electron interactions become larger, increasing as Z^3. In this respect the high-Z ions can act as nuclear probes in the same way that mesic atoms are currently used. The production of such ions is now feasible,[2,3] and we wish to note that the observability of hyperfine structure in their spectra is maximized if low-energy transitions of the type $1s2s$-$1s2p$ or $1s3l$-$1s3l'$ are studied, both because the wavelengths can fall in the visible or near-ultraviolet range and because the width of the hyperfine structure can be very large. This will apply to the odd-even or even-odd isotopes. The same transitions for isotopes which are not affected by hyperfine interaction can be useful for studies of Lamb shift and volume-isotope shift. This has also been pointed out by Accad, Pekeris, and Schiff.[4]

The $1snl$-$1snl'$ transitions have not yet been observed except in the lowest-Z atoms. Edlen and Lofstrand[5] have discussed the situation in their work on C V. Calculations of S-, P-, D-term energies have however been carried out by Weiss,[6] Sanders and Scherr,[7] Accad, Pekeris, and Schiff,[4] and Brown.[8] From the results of these workers one can obtain wavelengths accurate, in general, to within a few angstroms, which then allows us to make estimates of the nuclear effects and their observability. Well-known formulas are used here to compute the magnetic hyperfine parameter a_{1s}, spin-orbit parameters ζ_{nl}, first-order Lamb shifts $E_L(n,j)$, and the volume-isotope shifts $E_N(n,0)$, on the assumption of screened hydrogenic wave functions. The exchange electrostatic integrals $G_l(1s,nl)$ have also been computed using